J. Math. Biol. (1999) 38: 359–375

Journal of Mathematical Biology

Model and analysis of chemotactic bacterial patterns in a liquid medium

Rebecca Tyson[1], S. R. Lubkin[2], J. D. Murray[3]

[1]Department of Applied Mathematics, Box 352420, University of Washington, Seattle, WA 98195-2420, USA (rebecca@amath.washington.edu)
[2]Biomathematics Program, Box 8203, North Carolina State University, Raleigh, NC 27695-8203, USA (lubkin@eos.ncsu.edu)
[3]Department of Applied Mathematics, Box 352420, University of Washington, Seattle, WA 98195-2420, USA (murrayjd@amath.washington.edu).

Received: 10 March 1998 / Revised version: 7 June 1998

Abstract. A variety of spatial patterns are formed chemotactically by the bacteria *Escherichia coli* and *Salmonella typhimurium*. We focus in this paper on patterns formed by *E. coli* and *S. typhimurium* in liquid medium experiments. The dynamics of the bacteria, nutrient and chemoattractant are modeled mathematically and give rise to a nonlinear partial differential equation system.

We present a simple and intuitively revealing analysis of the patterns generated by our model. Patterns arise from disturbances to a spatially uniform solution state. A linear analysis gives rise to a second order ordinary differential equation for the amplitude of each mode present in the initial disturbance. An exact solution to this equation can be obtained, but a more intuitive understanding of the solutions can be obtained by considering the rate of growth of individual modes over small time intervals.

Key words: Chemotaxis – Partial differential equations – Bacteria – Mathematical Modeling – Pattern formation

Introduction

In this paper we present a simple and intuitively revealing mathematical analysis of transient solutions to a chemotaxis model involving partial differential equations. Our model equations are motivated by experiments performed by Budrene and Berg [3], in which they

observed patterns formed by *Escherichia coli* and *Salmonella typhimurium*. When placed in a liquid medium and exposed to intermediates of the tricarboxylic acid (TCA) cycle, the bacteria arrange themselves into high density aggregates. The patterns appear, rearrange and eventually fade on a time scale which is short compared with the generation time of the bacteria.

The simplest patterns are produced when the liquid medium contains a uniform distribution of bacteria and TCA cycle intermediate. Of the latter, succinate and fumarate produced the strongest effect. Only a small amount is necessary, as the bacteria are merely exposed to the TCA cycle intermediate as a stimulant, and do not rely on it as a carbon source. The initially uniform distribution of bacteria begins to form a stranded pattern of higher-density regions. Subsequently, the pattern resolves into discrete clumps of roughly uniform size over the entire surface of the liquid, though the pattern often starts in one general area and spreads from there. Over time the aggregates coalesce, thus becoming larger and decreasing in number. Ultimately the pattern dissipates and cannot be induced to re-form.

Fluid dynamic convection cells are not believed to be responsible for these patterns (H. C. Berg, personal communication); we hypothesize instead a primarily chemotactic mechanism. It is known that the bacteria secrete aspartate, a potent chemoattractant, in response to the stimulant. A chemoattractant is a chemical which the cells seek, in the sense that they move up gradients of that chemical. This process tends to increase the local cell density, while diffusion tends to do the opposite. The competition between the two processes is the driving force behind the patterns observed. Thus the main players in the experiments are the cells, the stimulant (succinate or fumarate) and the chemoattractant (aspartate).

The disappearance of the pattern is thought to be due to saturation of the chemotactic response. Since cellular production of chemoattractant is not countered by any form of chemoattractant degradation (or inhibition), the amount of chemoattractant in the dish increases continuously. As a result, the chemotactic response eventually saturates, and diffusion dominates.

We represent the experiments mathematically as a reaction-diffusion chemotaxis model. The numerical and analytic solutions of the equations verify our interpretation of the experimental results.

1 The model: a perturbation approach

Careful study of these experiments [3] has revealed that the biological processes most crucial in the formation of these bacterial patterns are

random migration and chemotaxis of bacteria. Also playing an important role is production of chemoattractant. There is no growth or death of cells over the brief time course of the liquid experiments, nor is there any uptake of aspartate by the cells as the liquid medium contains sufficient nutrient for the cells from other sources (E. O. Budrene, personal communication). We thus formulate a model consisting of two conservation equations

$$\begin{aligned} \frac{\partial n}{\partial t} &= D_n \nabla^2 n - \nabla \cdot \left[\frac{k_1 n}{(k_2 + c)^2} \nabla c \right] \\ \frac{\partial c}{\partial t} &= D_c \nabla^2 c + k_3 s \frac{k_4 n^2}{k_9 + n^2}. \end{aligned} \tag{1}$$

The variables n, c and s represent cell density, chemoattractant concentration, and nutrient concentration respectively. There is no equation for the nutrient in these experiments since so little of the nutrient is consumed. Thus, s is a parameter in this study. The terms on the right hand side represent, in order left to right and top to bottom, random and chemotactic cellular motion, chemoattractant diffusion, and chemoattractant production.

These equations are discussed in detail in [11]. We summarize the main points here. *E. coli* and *S. typhimurium* have been studied in detail and experimental results are available to aid in the selection of functional forms for the terms in equation (1). Diffusion coefficients for the random migration of cells [1, 2, 10] and chemotactic flux [5–7] have been measured by a number of researchers. For aspartate production, succinate is necessary, and the amount produced increases with the amount of succinate present [4]. Analysis of the parent model to the current one [11] shows that the production of aspartate must increase sufficiently quickly at low succinate concentrations. It must also saturate however, since the cells do not have unlimited capacity to produce aspartate, Thus, guided by the experimental data, we arrive at the mathematical model (in dimensionless form)

$$\begin{aligned} \frac{\partial u}{\partial t} &= d_u \nabla^2 u - \alpha \nabla \cdot \left[\frac{u}{(1 + v)^2} \nabla v \right] \\ \frac{\partial v}{\partial t} &= \nabla^2 v + w \frac{u^2}{\mu + u^2} \end{aligned} \tag{2}$$

where u, v and w represent cell density, chemoattractant concentration and succinate concentration respectively. In this paper we focus on the experiments where succinate is initially uniformly distributed and not

consumed. In this case w is constant. For our model analysis, presented below, we consider the one-dimensional situation, and generalise to two dimensions numerically. Zero flux boundary conditions are used throughout, in order to make the analysis and simulations consistent with the experiment.

The absence of growth and death in the cell population (over the time course of the experiment) gives the conservation equation

$$\int_0^l u(x, t)\, dx = u_0 l = l,$$

where u_o is the average initial nondimensional cell density. The parameter values are listed in Table 1 (dimensional) and Table 2 (dimensionaless). The parameter μ is unknown to us. The ratio of dimensionless time to dimensional time is unknown, by the Buckingham Pi theorem. The initial conditions of the experiment are uniform nonzero cell density and zero concentration of chemoattractant. So, from the nondimensionalization we have

$$u(x, 0) = 1 \quad \text{and} \quad v(x, 0) = 0.$$

Table 1. Known and estimated dimensional parameter values used in equations (1)

Parameter	Value	Source
k_1	$3.9 \times 10^{-9}\,\mathrm{Mcm^2 s^{-1}}$	Dahlquist, Lovely and Koshland, 1972
k_2	$5 \times 10^{-6}\,\mathrm{M}$	Dahlquist, Lovely and Koshland, 1972
k_3	Unknown	
k_4	Unknown	
k_9	Unknown	
D_n	$2\text{–}4 \times 10^{-6}\,\mathrm{cm^2\,s^{-1}}$	Berg and Turner, 1990; Berg, 1983 p93
D_c	$8.9 \times 10^{-6}\,\mathrm{cm^2\,s^{-1}}$	Berg 1983
D_s	$\approx 9 \times 10^{-6}\,\mathrm{cm^2\,s^{-1}}$	Berg 1983
n_0	$10^8\,\mathrm{cells\,ml^{-1}}$	Budrene and Berg, 1991
s_0	$1\text{–}3 \times 10^{-3}\,\mathrm{M}$	Budrene and Berg, 1995

Table 2. Known and estimated values for the dimensionless variables and parameters used in the study of the *E. coli* and *S. typhimurium* model, equations (2)

Variable	Initial value
u_0	1.0
w_0	1.0
v_0	0.0

Parameter	Value
α	80–90
d_u	0.25–0.5
μ	Unknown

We wish to find solutions of (2) which are oscillatory in space, and in time grow and then decay. This reflects the experimentally observed behaviour where, additionally, the observed wavenumbers decrease over time as the number of aggregates decreases. For simplicity we carry out the analysis for a one dimensional domain and then extrapolate the results to two dimensions.

A traditional linear analysis starts with a spatially and temporally uniform solution. From the equations it is clear that there is no such solution for which $u_0 \neq 0$. There is however, a spatially uniform solution which has the chemoattractant concentration increasing linearly with time,

$$\begin{aligned} u^*(x, t) &= 1 \\ v^*(x, t) &= \frac{1}{\mu + 1}\, t, \end{aligned} \tag{3}$$

with $v(x, 0) \equiv 0$ being the initial concentration of chemoattractant.

If we suppose that the initial conditions for (2) are small random perturbations about the initial cell density, we can look for solutions in the form

$$\begin{aligned} u(x, t) &= 1 + \varepsilon \sum_k f(t; k)\, \mathrm{e}^{ikx} \\ v(x, t) &= \frac{1}{\mu + 1}\, t + \varepsilon \sum_k g(t; k)\, \mathrm{e}^{ikx}. \end{aligned} \tag{4}$$

To approximate the actual experimental situation, where the initial concentration of chemoattractant is exactly zero, we set $g(0) = 0$. We may assume without loss of generality, $f(0) = 1$. The parameter ε (which is a measure of the size of the perturbation) satisfies $0 < \varepsilon \ll 1$ and so we are looking for spatially varying solutions superimposed on the temporally growing solution.

The wavenumber k and mode m of the solution are related by

$$k = \frac{m\pi}{l} \tag{5}$$

where l is the length of the domain in dimensionless units. Substituting (4) into (2) and linearising (in ε) in the usual way we obtain, for each k, the $O(\varepsilon)$ equations

$$\frac{dF(\tau)}{d\tau} = -d_u k^2 F(\tau) + \alpha(\mu + 1)^2 \frac{k^2}{\tau^2}\, G(\tau) \tag{6}$$

$$\frac{dG(\tau)}{d\tau} = -k^2 G(\tau) + \frac{2\mu}{(\mu + 1)^2}\, F(\tau) \tag{7}$$

where $\tau = \mu + 1 + t$ (note that $\tau_0 = \mu + 1 > 0$) and for a given k, $F(\tau) \equiv f(t; k)$, $G(\tau) \equiv g(t; k)$. The coefficient of the second term on the right hand side of (6) is the only one which depends on the chemotaxis parameter α.

It is clear from (6) that as $\tau \to \infty$ the coefficient of $G(\tau)$ tends to zero, and the solution for $F(\tau)$ reduces to a decaying exponential. Once this happens, the solution of (7) also gives a decaying exponential. So, with the forms (4) the mechanism accounts for ultimate pattern disappearance with time. This is also consistent with the original equations (2). Since the cells do not die (no death term in the first equation) and since the chemoattractant is produced but never degraded (no degradation term in the second equation), the chemoattractant concentration should continually increase. Thus, since the chemotaxis term is only large when v, the chemoattractant concentration, is small, the effect of chemotaxis will continually decrease until diffusion dominates. Let us now consider the temporary growth of spatial pattern from the initial disturbance.

For τ near τ_0 more insight can be gained by combining equations (6) and (7) to create a single second order differential equation for the amplitude of the cell density pattern, $F(\tau)$:

$$\frac{d^2F}{d\tau^2} + k^2\left((d_u + 1) + \frac{2}{\tau}\right)\frac{dF}{d\tau} + k^2\left(d_u k^2 + \frac{2d_u}{\tau} - \frac{2\alpha\mu}{\tau^2}\right)F = 0 \quad (8)$$

This equation has an exact solution in terms of hypergeometric functions

$$F(\tau) = \mathrm{e}^{-\frac{(1+A)\tau + C\ln(\tau)}{2}}\,\tau^{\frac{1+B}{2}}\left[K_2 \mathrm{H_U}\left(\frac{C}{2A} + \frac{1+B}{2}, 1 + B, A\tau\right) + K_1 \mathrm{H_{1F1}}\left(\frac{C}{2A} + \frac{1+B}{2}, 1 + B, A\tau\right)\right]$$

where

$$\begin{cases} A = k^2\,|d_u - 1| \\ B = \sqrt{1 + 8\alpha\mu k^2} \\ C = 2k^2(k^2(d_u + 1) - 2d_u) \end{cases}.$$

The special functions $\mathrm{H_U}$ and $\mathrm{H_{1F1}}$ are the confluent hypergeometric function and the Kummer confluent hypergeometric function respectively. This exact solution is not intuitively revealing, and so we use other approaches to obtain a clear understanding of the solution $F(\tau)$.

2 An analytic approximation

To begin the analysis, we make the assumption that the coefficients of the second order ordinary differential equation (8) change much less rapidly than the function itself and its derivatives. This lets us compare (8) to a constant coefficient second order equation over small intervals of τ. Denoting the coefficients of (8) by $\mathscr{D}(\tau)$ and $\mathscr{N}(\tau)$ we obtain

$$\frac{d^2F}{d\tau^2} + \mathscr{D}(\tau)\frac{dF}{d\tau} + \mathscr{N}(\tau)\,F = 0 \tag{9}$$

where

$$\mathscr{N}(\tau) = k^2\left(d_u k^2 + \frac{2d_u}{\tau} - \frac{2\alpha\mu}{\tau^2}\right) \tag{10}$$

$$\mathscr{D}(\tau) = k^2\left((d_u + 1) + \frac{2}{\tau}\right). \tag{11}$$

The last term in the bracketed expression in (10) is the only one in which α appears. The parameter μ appears explicitly only in that same term, but is also contained in the expression for τ and so its effect is not so easily isolated. Note that $D(\tau)$ is positive for all times τ greater than τ_0, while $N(\tau)$ can be positive, negative or zero for τ near τ_0. For all τ sufficiently large, $N(\tau) > 0$. Considering $N(\tau)$ and $D(\tau)$ constant for the moment, the solution of (9) over any sufficiently small τ intervals is of the form

$$\tilde{F}(\tau) = k_1 e^{\lambda_+ \tau} + k_2 e^{\lambda_- \tau}$$

where

$$\lambda_\pm = \tfrac{1}{2}\left(-\mathscr{D}(\tau) \pm \sqrt{\mathscr{D}(\tau)^2 - 4\mathscr{N}(\tau)}\right) \tag{12}$$

Since $\mathscr{D}(\tau) > 0\ \forall\tau$, we have $\mathrm{Re}(\lambda_-) < 0\ \forall\tau$. The sign of $\mathrm{Re}(\lambda_+)$ can vary however, and depends on the sign of $\mathscr{N}(\tau)$. When $\mathscr{N}(\tau) < 0$ for some k^2, $\mathrm{Re}(\lambda_+) > 0$ and the amplitude of that mode grows.

We focus our attention on how the chemotaxis coefficient α and the wavenumber k alter the solutions. If α is sufficiently large then $\mathscr{N}(\tau)$ will be negative for small values of τ, including τ_0. As τ increases, $\mathscr{N}(\tau)$ will increase through zero and become positive. The effect on λ_+ is to make the real part of the eigenvalue positive for small τ and negative for large τ. The point τ_{crit} at which λ_+ passes through zero is the same point at which $\mathscr{N}(\tau)$ becomes zero. Thus, for small τ, one component of $\tilde{F}$ is a growing exponential, while for larger τ both exponentials are decaying. We predict then, that α has a destabilising influence, that is, the growth of pattern becomes more likely as α increases.

For sufficiently large k^2, $N(\tau)$ becomes positive for all τ, resulting in solutions which are strictly decaying. Thus we would not expect to see wavenumbers larger than K, where

$$K^2 = \frac{2}{d_u(1+\mu)}\left(\frac{\alpha\mu}{1+\mu} - d_u\right) \tag{13}$$

is found by solving $N(\tau_0) = 0$. As time advances, fewer and fewer modes remain unstable, and as $\tau \to \infty$, the only unstable modes are those in a diminishing neighbourhood of 0. We can determine the fastest-growing wavenumber, K_{grow}, at any time by setting $\lambda_+(k^2) = 0 \equiv N(\tau) = 0$ and solving for k^2. This gives

$$K^2_{\text{grow}} = \frac{2}{\tau}\left(\frac{\alpha\mu}{d_u\tau} - 1\right)$$

which decreases with time. Thus we would not expect any wavenumber larger than K_{grow} to dominate the solution.

If our constant coefficient assumption is approximately correct over small but finite intervals of τ, then a series of solutions $\tilde{F}$ computed in sequential intervals $\Delta\tau$ could give rise to a solution which increases to a maximum and then decreases for all subsequent τ. The increasing portion would occur while λ_+ is positive. When we compute a numerical solution of the equation, we obtain the expected behaviour (Fig. 1). To obtain the numerical solution, we used the NAG stiff ODE solver D02NBF with set up routines D02NSF and D02NVF. The latter is the integrator set-up routine for Backward Differentiation Formulae.

We now construct an approximate analytic form for $F(\tau)$. The true location $\tau = \tau_{\text{crit}}$ of the maximum value of $F(\tau)$, $F_{\max}$, may be close to $\tilde{\tau}_{\text{crit}}$, where

$$N(\tilde{\tau}_{\text{crit}}) = 0 \;\Leftrightarrow\; \tilde{\tau}_{\text{crit}} = \frac{-1 + \sqrt{1 + \frac{2\alpha\mu}{d_u}k^2}}{k^2}. \tag{14}$$

We compare $\tilde{\tau}_{\text{crit}}$ with τ_{crit} obtained numerically; the results are shown in Fig. 2. The dotted line corresponds to $\tilde{\tau}_{\text{crit}}$ which we can compute for continuous values of k^2. The circles correspond to the numerically computed τ_{crit} at various values of k^2. The comparison is very close, and improves as k^2 and α increase.

The difference between $\tilde{\tau}_{\text{crit}}$ and τ_{crit} gives an indication of the size of $d^2F/d\tau^2$ at τ_{crit}. By definition, τ_{crit} is the time at which $dF/d\tau = 0$ and so (9) reduces to

$$\left.\frac{d^2F}{d\tau^2}\right|_{\tau_{\text{crit}}} = -N(\tau_{\text{crit}})F.$$

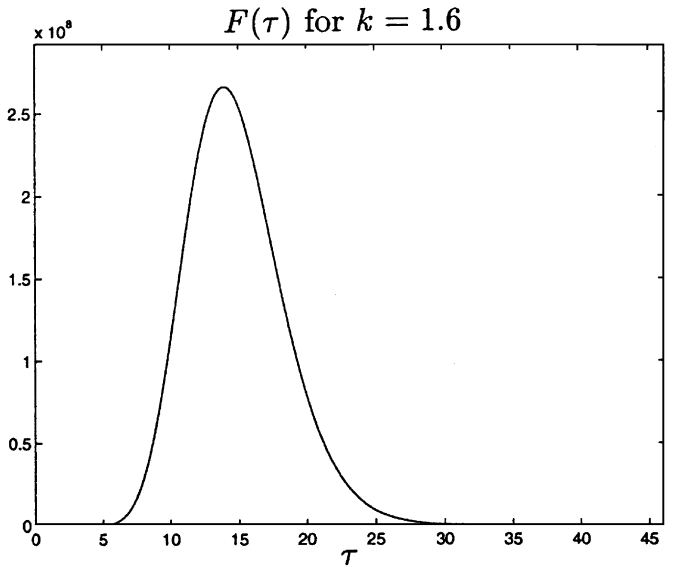

Fig. 1. The amplitude F(τ) of the $k = 1.6$ perturbation of the initial uniform cell density. The other parameter values are: $d_u = 0.33$, $\alpha = 80$, $\mu = 1$, $u_0 = 1$, $w = 1$ and $l = 10$

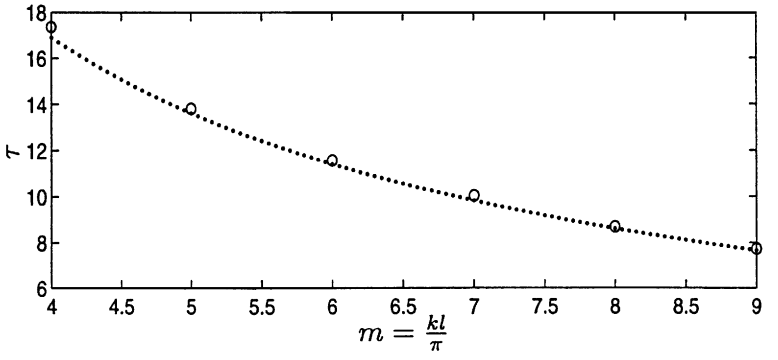

Fig. 2. Comparison of τ_{crit} (circles) and $\tilde{\tau}_{\text{crit}}$ (predicted τ_{crit}) (dotted line) plotted against wavenumber. Parameter values are $\alpha = 80$, $d_u = 0.33$, $\mu = 1$, $u_0 = 1$, $w = 1$ and $l = 10$

Since the second derivative of a function is always less than zero at a maximum we know that $N(\tau_{\text{crit}})$ is positive. Thus τ has already increased past the point where $N(\tau)$ changes sign, and $\tilde{\tau}_{\text{crit}}$ gives us a minimum estimate for τ_{crit}. From Fig. 2 we see that $\tilde{\tau}_{\text{crit}}$ and τ_{crit} are reasonably close, which suggests that $N(\tau_{\text{crit}})$ may be close to zero. In turn, this indicates that $d^2F/d\tau^2$ may be numerically small at the maximum, $F_{\max}$.

We are thus encouraged to solve equation (9) with the second derivative term omitted, and compare the approximate solution with the numerical one. After some straightforward algebra we find the solution of the first order ordinary differential equation to be

$$F_1(\tau) = \left[\frac{(d_u+1)k^2\tau_0 + 2}{(d_u+1)k^2\tau + 2}\right]^{\frac{2\alpha\mu k^2}{2} - \frac{2d_u(d_u+1-2)}{(d_u+1)^2}} \left[\frac{\tau}{\tau_0}\right]^{\frac{2\alpha\mu k^2}{2}} e^{\frac{d_u}{d_u+1}k^2(\tau_0-\tau)}. \qquad (15)$$

Plots of the first order and second order equation solutions $F(\tau)$ and $F_1(\tau)$ are shown in Fig. 3. For this figure α was set to 30, since the two curves have such disparity in magnitude for $\alpha = 80$ that they cannot be viewed on the same coordinate grid. The observations below apply equally however, for the larger value of α.

At first glance we notice the marked difference in the height of the two functions. Apart from this difference however, the two functions have many similarities: (1) the peaks occur at approximately the same value of τ, (2) the peak interval, defined as the time during which $F(\tau) > F(\tau_0)$, is about the same, especially for the lower frequencies, and (3) the two curves appear to be similarly skewed to the left. Increasing α results in a large increase in both $F_{\max}$ and $F_{1_{\max}}$, but doesn't change the slope. The two solutions are also similar with respect to the behaviour of the different modes investigated. The larger the value of k^2, the earlier τ_{crit} is reached, and the shorter the interval over which F or F_1 is larger than the initial value F_0.

If we normalise the data for $F(\tau)$ and $F_1(\tau)$ so that it lies in the interval [0, 1] we see that the two solutions map almost directly on top of each other (Fig. 4). The main difference therefore, between the approximate solution and the exact solution (obtained numerically) is

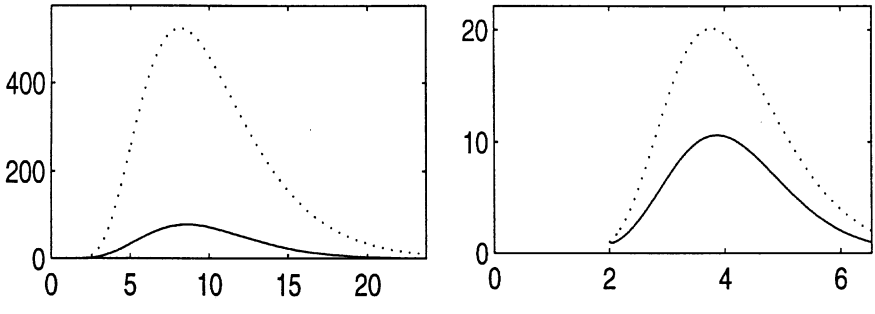

Fig. 3. $F(\tau)$ (solid line) and $F_1(\tau)$ (dotted line) plotted together against τ for $\alpha = 30$ and various values of k. The other parameter values are as listed in Fig. 2

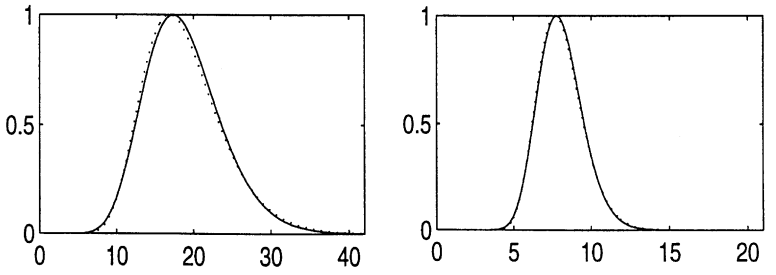

(a) $k = 1.3$ (b) $k = 2.8$

Fig. 4. The solutions $F(\tau)$ (solid line) and $F_1(\tau)$ (dotted line) plotted against τ and normalised to lie between 0 and 1. The parameter values are as listed in Fig. 2

simply in a scaling factor. This scaling factor is very large, suggesting that the second order derivative term is not small outside the neighbourhood of the maximum.

At this stage we have an intuitive understanding of the solutions $F(\tau)$ of equation (8). We also have an approximate analytic solution, $F_1(\tau)$, which we can use to predict the effect of changing various parameters.

3 Interpretation of results

In terms of the model equations, we are particularly interested in predicting the size and number of aggregates which will form, and the length of time during which they will be visible, that is, when $F(\tau)$ is sufficiently large. If nonlinear effects are not too strong, we expect that the number of aggregates will be determined by the combined effect of the solutions corresponding to the various modes.

Numerical results are shown in Fig. 5. We observe that there is one wavenumber which attains a higher amplitude than any other. We refer to this wavenumber as $k_{\max}$ (here $k_{\max} = 2.20$). We also note that every wavenumber k larger than $k_{\max}$ initially has a slightly higher growth rate than $k_{\max}$. These high frequencies quickly begin decaying however, while the amplitude of the $k_{\max}$ pattern is still growing rapidly.

Once the $k_{\max}$ solution begins to decay, solutions corresponding to smaller wavenumbers become largest in decreasing order. The amplitude of each solution with $k < k_{\max}$ is always in the process of decaying, once it supersedes the next highest mode. Thus we should see a continuous decrease in the wavenumber of the observed pattern as

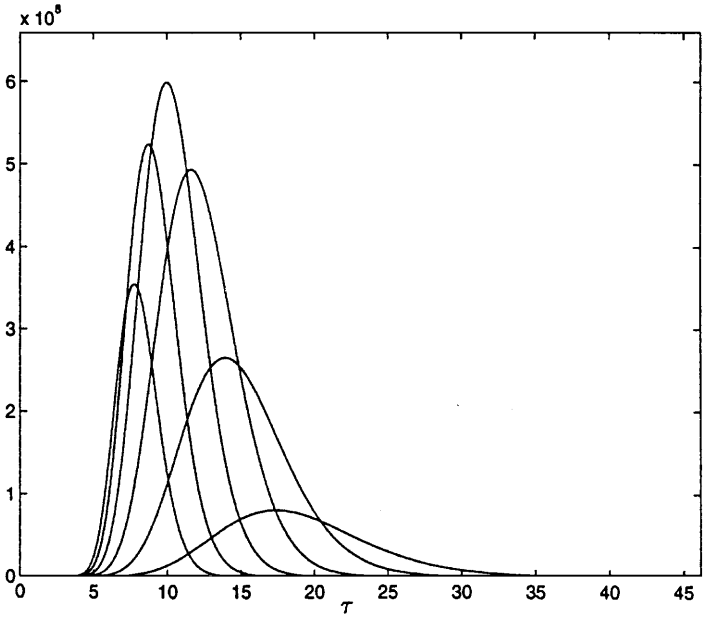

Fig. 5. F(τ) for discrete values of $k = m\pi/l$, $m = 4$ to 9 (or $k = 1.26$ to 2.83). The $m = 9$ curve decays the fastest, then the $m = 8$ curve, etc. The curve corresponding to $m = 7$ has the highest peak. The other parameter values are: $d_u = 0.33$, $\alpha = 80$, $\mu = 1$, $u_0 = 1$, $w = 1$ and $l = 10$. ($K = 10.9$)

t increases, accompanied by a decrease in amplitude. This corresponds to the biologically observed coalescing of aggregates and eventual dissipation of pattern. Note that for these figures $K_{\text{grow}} = 5.47$ and so $k_{\max}$ is less than K_{grow} by a factor of 2. For all of the numerical solutions observed in this study, $k_{\max}$ was consistently much less than K_{grow}.

4 Numerical simulation results

We can now compare the predictions of the linear theory with the actual solution behaviour of the partial differential equations. Simulation results were obtained using Strang Splitting and Clawpack [8, 9]. The method and its behaviour is discussed in detail in Tyson et al. [12]. For all of the simulations, zero flux boundary conditions were used. The initial condition in chemoattractant concentration is zero everywhere on the domain, and in cell density is a random perturbation about $u_0 = 1$. The random perturbation was obtained via the Fortran random number generator routine, rand, which produces pseudo-random real numbers distributed uniformly over (0, 1). Various seeds

and grid refinements were used. The results presented in the figures below are all generated from runs using the same seed, grid spacing ($\Delta x = 0.06$) and noise amplitude (order 10^{-1}).

A time sequence for $\alpha = 80$ is shown in Fig. 6. The sequence was truncated at the time beyond which little change was observed in the number of peaks, and the pattern amplitude simply decreased. The plots in the left hand column of each figure are the cell density profiles at various times τ, while the plots in the right hand column are the corresponding power spectral densities. The density axis for the latter plots are restricted to lie above the mean value of the initial power spectral density, at $\tau = \tau_0$. This highlights the pattern modes which grow.

As predicted in equation (13), the power spectral density plots indicate that spatial pattern modes with wavenumber higher than $K = 10.9$ do not grow. Also, spread of "nonzero" modes decreases as time increases. In the actual cell density distribution, the pattern observed initially has many peaks, and the number of these decreases over time. Our prediction for the value of $k_{\max}$ is off by a factor of two in these figures. The solution is actually dominated by $k_{\max} \approx 1.1$ while the predicted value was 2.2.

Moving to two dimensional simulations, we obtain the same type of results from the model as was observed in the one dimensional case. An initial condition consisting of small random perturbations about a uniform distribution of cells produces patterns consisting of a random arrangement of spots (Fig. 7). From the surface plot, Fig. 8, it is clear that the aggregates of cells are very dense in comparison to the regions in between. The number of spots is large at first and then decreases over time as neighbouring spots coalesce. Eventually, all of the spots disappear.

Recall that this is exactly what is observed in the bacterial experiments. To begin with, bacteria are added to a petri dish containing a uniform concentration of succinate. The mixture is well-stirred, and then allowed to rest. At this point, the state of the solution in the petri dish is mimicked by the initial condition for our model: small perturbations of a uniform distribution of cells and succinate. After a short period of time, on the order of 20 minutes, the live bacteria aggregate into numerous small clumps which are very distinct from one another. This behaviour corresponds to the random arrangement of spots separated by regions of near-zero cell density observed in the model solutions. Experimentally, the bacterial aggregates are seen to join together, forming fewer and larger clumps. This also is present in the mathematical model, and is clearly evident when the solutions are displayed as a movie with the frames separated by small time

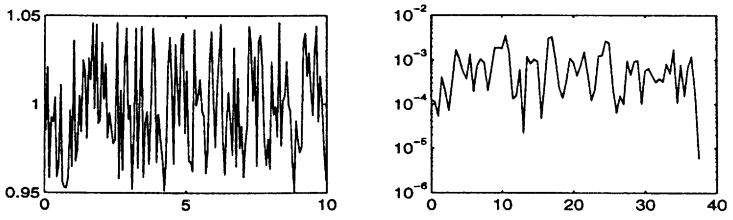

(e) $\tau = 2$

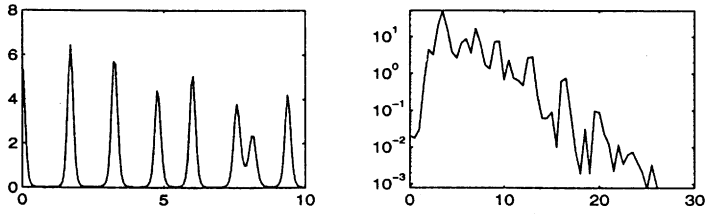

(f) $\tau = 2.6$, $k_{max} = 1.1$

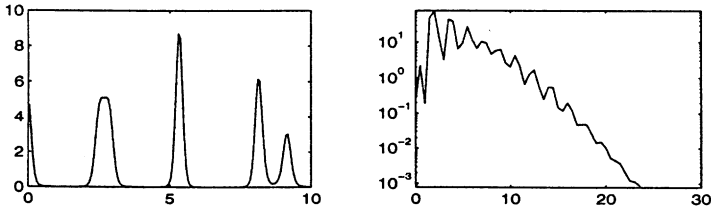

(g) $\tau = 3.7$, $k_{max} = 0.6$

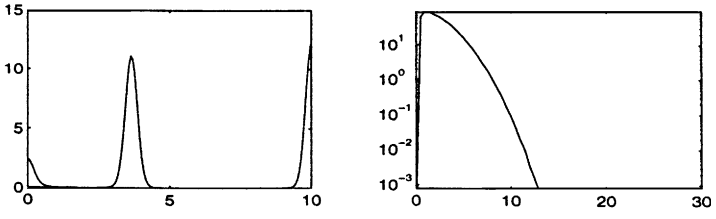

(h) $\tau = 10$, $k_{max} = 0.3$

Fig. 6. *Left-hand plots*: cell density plotted against space at various points in time. *Right-hand plots*: corresponding power spectral density functions. Initially the cells are uniformly distributed over the one dimensional domain and disturbed with a small perturbation of order 1×10^{-1}. Parameter values are the same as for Fig. 5: $d_u = 0.33$, $u_0 = 1$, $w_0 = 1$, $l = 10$, $\mu = 1$ and $\alpha = 80$. ($K = 10.9$)

Fig. 8. Surface plot of the cell density pattern arising from a uniform distribution of stimulant on a square domain. This output corresponds to the $t = 2$ image plot in Fig. 7

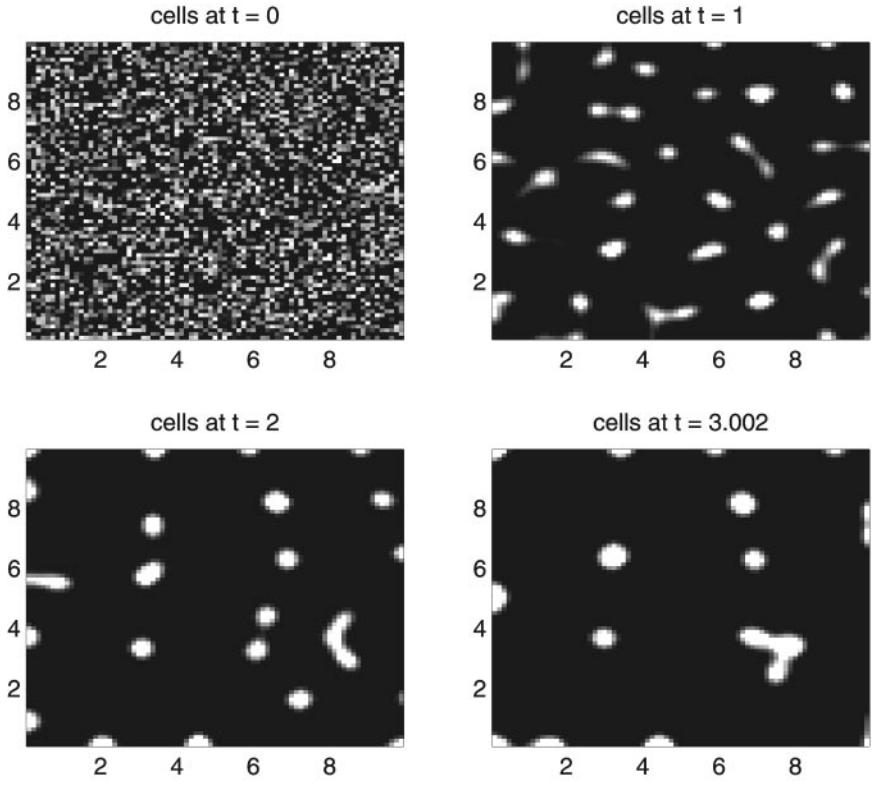

Fig. 7. Two dimensional cell density pattern arising from a uniform distribution of stimulant on a square domain. White corresponds to high cell density, black to low cell density. Parameter values: $d_u = 0.33$, $\alpha = 80$, $\mu = 1$, $u_0 = 1$, $w = 1$ and $l = 10$

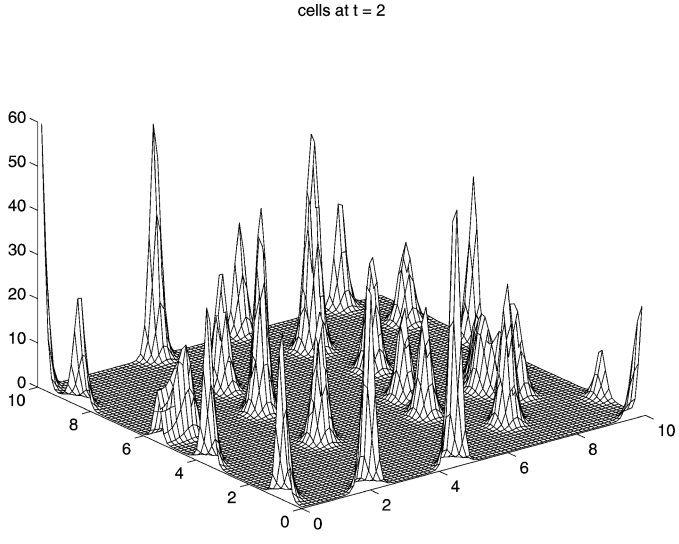

increments. In both the model and experiment, the spots eventually disappear and cannot be induced to re-form. This is explained by the mathematical model as a saturation of the chemotactic response, which no longer has any effect as the production of chemoattractant increases continually.

5 Conclusions

In this paper, we explored a simple and intuitively revealing analysis which explains how evolving patterns of randomly arranged spots appear transiently in a chemotaxis model and in experiment. The central idea is to consider the rate of growth of individual modes over small time intervals, and extrapolate from this to the combined behaviour of all disturbance frequencies. Low mode number perturbations to the uniform solution are unstable and grow in magnitude, but eventually these stabilize and decay with the larger mode numbers stabilizing first. This agrees qualitatively, and to a great extent quantitatively, with what is observed experimentally and numerically: clumps form, coalesce into larger aggregates, and eventually disappear.

Acknowledgements. We thank Julian Cook for his helpful contributions to this project. This work has been supported in part by NSF grants DMS-9306108 (SRL) and DMS-9500766 (SRL, JDM), and by NSERC scholarships PGSA and PGSB (RT).

References

1. H. C. Berg and L. Turner. Chemotaxis of bacteria in glass capillary arrays. Biophys. J., 58: 919–930, 1990
2. Howard C. Berg. Random Walks in Biology. Princeton University Press, Princeton, NJ, 1983
3. E. O. Budrene and H. C. Berg. Complex patterns formed by motile cells of escherichia coli. Nature, 349(6310): 630–633, 1991
4. E. O. Budrene and H. C. Berg. Dynamics of formation of symmetrical patterns by chemotactic bacteria. Nature, 376 (6535): 49–53, 1995
5. F. W. Dahlquist, P. Lovely, and Koshland, Jr, D. E. Qualitative analysis of bacterial migration in chemotaxis. Nat. New Biol., 236: 120–123, 1972
6. R. M. Ford and D. A. Lauffenburger. Analysis of chemotactic bacterial distributions in population migration assays using a mathematical model applicable to steep or shallow attractant gradients. Bulletin of Mathematical Biology, 53(5): 721–749, 1991
7. R. Lapidus and R. Schiller. Model for the chemotactic response of a bacterial population. Biophys. J., 16: 779–789, 1976

8. R. J. LeVeque. CLAWPACK software. available from netlib.att.com in netlib/pdes/claw or on the Web at the URL http: //www.amath.washington. edu/ ~ rjl/clawpack.html
9. R. J. LeVeque. CLAWPACK USER NOTES. available from netlib.bell-labs.com in netlib/pdes/claw/doc or at http://www.amath.washington.edu/ ~ rjl/clawpack.html
10. B. R. Phillips, J. A. Quinn, and H. Goldfine. Random motility of swimming bacteria: Single cells compared to cell-populations. AIChE Journal, 40: 334–348, 1994
11. R. Tyson, S. R. Lubkin, and J. D. Murray. A minimal mechanism of bacterial pattern formation. Proc. Roy. Soc. B (in press, 1999)
12. R. Tyson, L. G. Stern, and R. J. LeVeque. Fractional step methods applied to a chemotaxis model. Journal of Mathematical Biology (in press, 1999)